

# EXPLORING NEW FEATURES OF NEUTRINO OSCILLATIONS WITH VERY LOW ENERGY MONOENERGETIC NEUTRINOS

J.D. Vergados<sup>1</sup>, and Yu.N. Novikov<sup>2</sup>

*1 University of Ioannina,  
Ioannina, GR 45110, Greece*

*E-mail: Vergados@cc.uoi.gr and*

*2 Petersburg Nuclear Physics Institute, 188300, Gatchina, Russia*

(Dated: November 18, 2018)

In the present work we propose to study neutrino oscillations employing sources of monoenergetic neutrinos following electron capture by the nucleus. Since the neutrino energy is very low the smaller of the two oscillation lengths,  $L_{23}$ , appearing in this electronic neutrino disappearance experiment can be so small that the full oscillation can take place inside the detector and one may determine very accurately the neutrino oscillation parameters. Since in this case the oscillation probability is proportional to  $\sin^2 2\theta_{13}$ , one can measure or set a better limit on the unknown parameter  $\theta_{13}$ . This is quite important, since, if this mixing angle vanishes, there is not going to be CP violation in the leptonic sector. The best way to detect it is by measuring electron recoils in neutrino-electron scattering. One, however, has to pay the price that the expected counting rates are very small. Thus one needs a very intensive neutrino source and a large detector with as low as possible energy threshold and high energy and position resolution. Both spherical gaseous and cylindrical liquid detectors are studied. Different source candidates are considered.

PACS numbers: 13.15.+g, 14.60Lm, 14.60Bq, 23.40.-s, 29.25.Rm, 95.55.Vj.

## INTRODUCTION.

The discovery of neutrino oscillations can be considered as one of the greatest triumphs of modern physics. It began with atmospheric neutrino oscillations [1] interpreted as  $\nu_\mu \rightarrow \nu_\tau$  oscillations, as well as  $\nu_e$  disappearance in solar neutrinos [2]. These results have been recently confirmed by the KamLAND experiment [3], which exhibits evidence for reactor antineutrino disappearance. As a result of these experiments we have a pretty good idea of the neutrino mixing matrix and the two independent quantities  $\Delta m^2$ , e.g.  $|m_2^2 - m_1^2|$  and  $|m_3^2 - m_2^2|$ . Fortunately these two  $\Delta m^2$  values are vastly different,

$$\Delta m_{21}^2 = |m_2^2 - m_1^2| = (7.65_{-0.20}^{+0.23}) \times 10^{-5} (eV)^2$$

and

$$\Delta m_{32}^2 = |m_3^2 - m_2^2| = (2.4_{-0.11}^{+0.12}) \times 10^{-3} (eV)^2.$$

This means that the relevant  $L/E$  parameters are very different. Thus for a given energy the experimental results can approximately be described as two generation oscillations. For an accurate description of the data, however, a three generation analysis [4],[5] is necessary.

In all of these analyses the oscillation length is much larger than the size of the detector. So one is able to see the effect, if the detector is placed in the right distance from the source. It is, however, possible to design an experiment with an oscillation length of the order of the size of the detector. In this case one can start with zero oscillation near the source, proceed to maximum oscillation near the middle of the detector and end up again with no oscillation on the other end. This is achieved, if one considers a neutrino source with as low as practical neutrino energy. The main requirements are as follows:

- The neutrinos should have as low as possible energy so that the oscillation length can be minimized. At the same time it should not be too low, so that the neutrino-electron cross section is sizable.
- A monoenergetic source has the advantage that some of the features of the oscillation patterns are not washed out by the averaging over a continuous neutrino spectrum.

- The life time of the source should be suitable for the experiment to be performed. If it is too short, the time available will not be adequate for the execution of the experiment. If it is too long, the number of counts during the data taking will be too small. Then one will face formidable backgrounds and/or large experimental uncertainties.
- The source should be cheaply available in large quantities.

Clearly a compromise has to be made in the selection of the source. It appears, unfortunately, that the oscillation length one may have to live with, may be quite a bit longer than that of the previously considered triton source with a maximum energy of 18.6 keV, i.e. an average oscillation length is 6.5m.

At such low energies the only neutrino detector, which is sensitive to neutrino oscillations, is one, which is capable of detecting recoiling electrons. With this detector one is sensitive to all neutrino flavors [6], [7]. In fact one can detect:

- electrons which are produced by electron neutrinos via both the charged and the neutral current interaction. These will manifest as **electron neutrino disappearance**
- electrons are produced from the other two neutrino flavors due to the neutral current interaction. These two flavors are due to the **muon and tau neutrino appearance**.

Since the importance of the cross section due to the charged current relative to that due to the neutral current depends on the electron energy, one has a novel feature, i.e. the effective oscillation probability depends on the electron energy. Thus the results may appear as disappearance oscillation in some kinematical regime and as appearance oscillation in some other regime. In this paper we will examine how these features can best be exploited in determining the neutrino oscillation parameters.

## ELASTIC NEUTRINO ELECTRON SCATTERING

For low energy neutrinos the historic process neutrino-electron scattering [6] [7] is very useful. The differential cross section [8] takes the form

$$\frac{d\sigma}{dT} = \left(\frac{d\sigma}{dT}\right)_{weak} + \left(\frac{d\sigma}{dT}\right)_{EM} \quad (1)$$

The second term, due to the neutrino magnetic moment, is inversely proportional to the electron energy and, at the low electron energies of the present set up, may be used in improving the current limit of the neutrino magnetic moment by two orders of magnitude. It is not, however, the subject of the present study, which is concerned with neutrino oscillations. The cross section in the rest frame of the initial electron due to weak interaction alone becomes:

$$\begin{aligned} \left(\frac{d\sigma}{dT}\right)_{weak} &= \frac{G_F^2 m_e}{2\pi} [(g_V + g_A)^2 \\ &+ (g_V - g_A)^2 \left[1 - \frac{T}{E_\nu}\right]^2 + (g_A^2 - g_V^2) \frac{m_e T}{E_\nu^2}] \end{aligned} \quad (2)$$

$$g_V = 2 \sin^2 \theta_W + 1/2 \quad (\nu_e), \quad g_V = 2 \sin^2 \theta_W - 1/2 \quad (\nu_\mu, \nu_\tau)$$

$$g_A = 1/2 \quad (\nu_e), \quad g_A = -1/2 \quad (\nu_\mu, \nu_\tau)$$

For antineutrinos  $g_A \rightarrow -g_A$ .

The scale is set by the weak interaction:

$$\frac{G_F^2 m_e}{2\pi} = 4.45 \times 10^{-48} \frac{cm^2}{keV} \quad (3)$$

The above equation must be modified, if one wishes to include the fact that the initial electron is bound. For neutrino energies in the tens of keV, however, it has been shown by Gounaris, Paschos and Porfyriadis [9] that such a modification lowers the cross section by no more than 10%. So we are not going to consider such effects here.

The electron energy depends on the neutrino energy and the scattering angle and is given by:

$$T = \frac{2 m_e (E_\nu \cos \theta)^2}{(m_e + E_\nu)^2 - (E_\nu \cos \theta)^2} \quad (4)$$

The last equation for sufficiently low energies can be simplified as follows:

$$T \approx \frac{2(E_\nu \cos \theta)^2}{m_e} \quad (5)$$

The maximum electron energy depends on the neutrino energy squared. The total cross section as a function of neutrino energy is shown in Fig. 1.

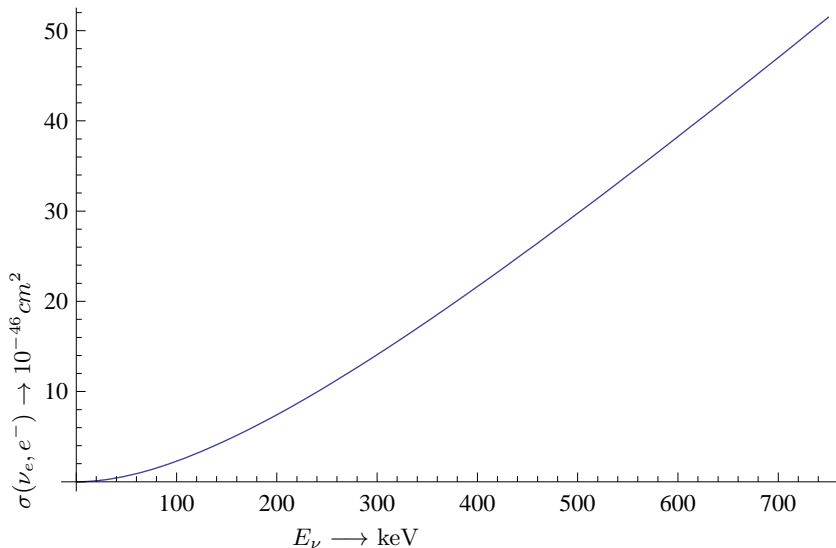


FIG. 1: The total  $(\nu_e, e^-)$  cross section in the absence of oscillations as a function of the neutrino energy. In the present work the neutrinos have a definite energy.

### NEUTRINO SHORT BASELINE OSCILLATIONS

The electron neutrino, produced in weak interactions, can be expressed in terms of the three mass eigenstates as follows:

$$\nu_e = \cos \theta_{12} \cos \theta_{13} \nu_1 + \sin \theta_{12} \cos \theta_{13} \nu_2 + \sin \theta_{13} e^{i\delta} \nu_3 \quad (6)$$

Then the  $\nu_e$  disappearance oscillation probability is given by:

$$\begin{aligned} P(\nu_e \rightarrow \nu_e) = & 1 - [\cos^4 \theta_{13} \sin^2 2\theta_{12} \sin^2 (\pi \frac{L}{L_{21}}) \\ & + \sin^2 \theta_{12} \sin^2 2\theta_{13} \sin^2 (\pi \frac{L}{L_{32}}) \\ & + \cos^2 \theta_{12} \sin^2 2\theta_{13} \sin^2 (\pi \frac{L}{L_{31}})] \end{aligned} \quad (7)$$

with

$$L_{ij} = \frac{4\pi E_\nu}{m_i^2 - m_j^2} \quad (8)$$

$\sin\theta_{13}$  is a small quantity constrained by the CHOOZ experiment and it will be further investigated below. In the limit in which it is neglected, one recovers the standard expression familiar from the solar neutrino oscillation analysis, if we take  $s_{12} \approx \sin\theta_{solar}$ ,  $c_{12} \approx \cos\theta_{solar}$ ,  $\theta_{solar}$  as determined from the solar neutrino data. Assuming  $\Delta m_{31}^2 \approx \Delta m_{32}^2$  we find:

$$P(\nu_e \rightarrow \nu_e) \approx 1 - [(\sin 2\theta_{solar})^2 \sin^2(\pi \frac{L}{L_{21}}) + \sin^2(2\theta_{13}) \sin^2(\pi \frac{L}{L_{32}})] \quad (9)$$

where the term proportional to  $\sin^2(2\theta_{13})$ , connected with the small oscillation length [10]  $L_{32}$ , ( $L_{21} \approx 32L_{32}$ ), is relevant for the experimental approaches discussed in the present paper. As we have already mentioned in connection with the NOSTOS experiment[10], in addition to the electronic neutrinos, which are depleted by the oscillations, is sensitive to the other two neutrino flavors, which can also produce electrons via the neutral current interaction. These flavors are generated via the appearance oscillation:

$$P(\nu_e \rightarrow \sum_{\alpha \neq e} \nu_\alpha) \approx (\sin 2\theta_{solar})^2 \sin^2(\pi \frac{L}{L_{21}}) + \sin^2(2\theta_{13}) \sin^2(\pi \frac{L}{L_{32}}) \quad (10)$$

Thus the number of the scattered electrons, which bear this rather unusual oscillation pattern, is proportional to the  $(\nu_e, e^-)$  scattering cross section with a proportionality constant  $C(E_\nu, T)$  given by:

$$C(E_\nu, T) = 1 - \chi(E_\nu, T) \left[ (\sin 2\theta_{solar})^2 \sin^2(\pi \frac{L}{L_{21}}) + \sin^2(2\theta_{13}) \sin^2(\pi \frac{L}{L_{32}}) \right]. \quad (11)$$

The function  $\chi(E_\nu, T)$ , which represents the relative difference between the cross section of the electronic neutrino and its other two flavors, has been previously discussed [10].

### GEOMETRIC CONSIDERATIONS

The total neutrino electron scattering cross section as a function of  $x$  and  $L$  can be cast in the form:

$$\sigma(L, x) = \sigma(0, x) (1 - \chi(x)p(L, x)) \quad (12)$$

with  $x = \frac{E_\nu}{m_e}$  and

$$\sigma(0, x) = \frac{G_F^2 m_e^2 x^2 (17.7464x^2 + 15.3098x + 3.36245)}{2\pi (2x + 1)^3} \quad (13)$$

is the total cross section in the absence of oscillations. Furthermore

$$p(L, x) = \sin^2 \left( \frac{0.0595922L}{330x} \right) \sin^2(2\theta_{solar}) + \sin^2 \left( \frac{0.0595922L}{10x} \right) \sin^2(2\theta_{13}) \quad (14)$$

with  $L$  the source detector distance in meters and

$$\chi(x) = \frac{2.8664x^2 + 4.1498x + 1.50245}{17.7464x^2 + 15.3098x + 3.36245} \quad (15)$$

We will assume that the volume of the source is much smaller than the volume of the detector.

We will consider two possibilities:

### Spherical detector with the source at the origin

The number of events between  $L$  and  $L + dL$  is given by:

$$dN = N_\nu n_e \frac{4\pi L^2 dL}{4\pi L^2} \sigma(L, x) = N_\nu n_e dL \sigma(L, x) \quad (16)$$

or

$$\frac{dN}{dL} = N_\nu n_e \sigma(L, x) \quad (17)$$

To compare with other geometries we rewrite this as follows:

$$\frac{dN}{d\rho} = R_0 N_\nu n_e \sigma(x, \rho) \quad (18)$$

or

$$\frac{dN}{d\rho} = \frac{G_F^2 m_e^2}{2\pi} R_0 N_\nu n_e g_s(\rho) \tilde{\sigma}(x, \rho), \quad g_s(\rho) = 1 \quad (19)$$

with  $N_\nu$  the number of neutrinos emitted by the source,  $n_e$  the density of electrons in the target,  $R_0$  the radius of the target and  $\rho = L/R_0$ .  $\tilde{\sigma}(x, \rho)$  is the neutrino - electron cross section in units of  $G_F^2 m_e^2 / 2\pi$ . The geometry factor  $g_s(\rho)$  is in this case unity.

### Cylindrical detector with the source at the center of one of its basis

The number of events between  $r$  and  $r + dr$  and  $z$  and  $z + dz$  is now given by:

$$dN = N_\nu n_e \frac{2\pi r dr dz}{4\pi(r^2 + z^2)} \sigma(x, \sqrt{r^2 + z^2}) \quad (20)$$

which yields

$$\frac{dN}{d\rho d\zeta} = N_\nu n_e R \frac{1}{2} \frac{u\rho}{\zeta^2 + u^2\rho^2} \sigma(x, \frac{R}{u} \sqrt{\zeta^2 + u^2\rho^2}), \quad (21)$$

where  $R$  is the radius of the cylinder,  $u = R/h$  ( $h$  is the length of the cylinder),  $\rho = r/R$  and  $\zeta = z/h$ . This can be written as

$$\frac{dN}{d\rho d\zeta} = \Lambda g_c(\rho, \zeta, u, R) \frac{1}{2} \tilde{\sigma}(x, \frac{R}{u} \sqrt{\zeta^2 + u^2\rho^2}), \quad (22)$$

$$g_c(\rho, \zeta, u, R) = \frac{u\rho}{\zeta^2 + u^2\rho^2}, \quad \Lambda = \frac{G_F^2 m_e^2}{2\pi} R N_\nu n_e \quad (23)$$

Note that the geometric factor  $g_c(\rho, \zeta, u, R)$ , which is absent in the spherical geometry, in this case is less than unity.

It is instructive to compare the two geometries in the absence of oscillations. In such a case we find that the number of events is given by:

$$N_c = N_\nu n_e R \sigma(x, 0) \frac{1}{4} \left( 2 \tan^{-1} \left( \frac{1}{u} \right) + \frac{\log(u^2 + 1)}{u} \right) \quad (24)$$

while for a half sphere of the same volume we find:

$$N_s = N_\nu n_e R \sigma(x, 0) \frac{\sqrt[3]{\frac{3}{2}}}{2\sqrt[3]{u}} \quad (25)$$

The relative merit  $N_c/N_s$  is shown in Fig. 2. This ratio becomes unity for  $u = 1.12$ , which is much larger than the value of 11/91 of the planned detector. Note, however, that for  $u=11/91$  the relative merit is 0.75, i.e. not far from unity.

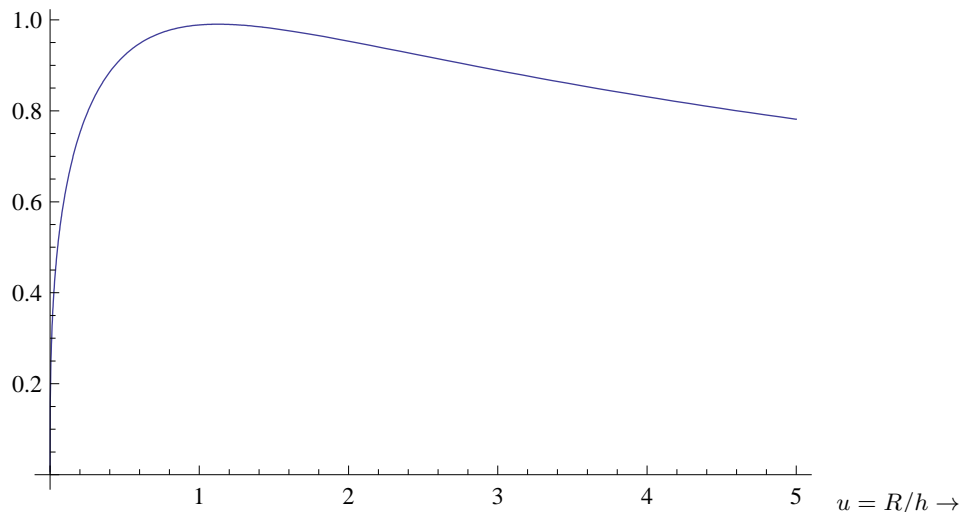


FIG. 2: The relative geometric merit,  $N_c/N_s$ , of a cylinder compared to that of a half sphere of the same volume as a function of  $u = R/h$

## CANDIDATES FOR NEUTRINO OSCILLOMETRY

One can ask whether the relevant candidates for small length oscillation measurements exist in reality. The analysis of known information on nuclides show that there are many cases with a small neutrino energy in the orbital electron capture by nucleus. Since this process has the two-body mechanism, the total neutrino energy is equal to the difference of the total capture energy  $Q_{EC}$  and binding energy of captured electron  $B_i$  :

$$Q_\epsilon = Q_{EC} - B_i \quad (26)$$

This value can be easily determined because the capture energies are usually known (or can be measured very precisely by the ion-trap spectrometry [11]) and the electron binding energies are tabulated [12]. The main feature of the electron capture process is the monochromaticity of neutrino. This paves the way for the neutrino oscillometry, which is introduced below. Table I shows the relevant nuclides, which emit monoenergetic neutrinos with energy less than 750 keV, half-life not more than  $10^5$  y, and whose production rates in the neutron reactors can provide rather high intensity of neutrinos ( $\geq 10^{12} \text{ s}^{-1}$ ). Columns 2-4 of Table I show the decay characteristics of the corresponding nuclides, column 5 gives a half value of the small oscillation length  $L_{32}$ , column 6 shows

the recoil electron maximal energy in the neutrino scattering on electron, and column 7 presents the masses of samples that can reasonably be produced by irradiation of natural targets in reactors with the assumed neutron flux of  $5 \times 10^{14} \text{cm}^{-2} \text{s}^{-1}$  and known neutron capture cross-sections for individual nuclides. We can see from Table I that there is a variety of nuclides with different half-lives and capture energies. Short half-life nuclides, as e.g.  $^{51}\text{Cr}$ ,  $^{55}\text{Fe}$ ,  $^{71}\text{Ge}$ , and  $^{103}\text{Pd}$ , have an advantage in the sense that they can be rapidly produced in reactors, whereas long-lived ones, as  $^{41}\text{Ca}$ ,  $^{157}\text{Tb}$ ,  $^{163}\text{Ho}$  and  $^{193}\text{Pt}$  need long-term irradiation in order to accumulate necessary decay intensity. The nuclides  $^{157}\text{Tb}$  and  $^{163}\text{Ho}$  can be accumulated after disintegration of  $^{157}\text{Dy}$  and  $^{163}\text{Er}$ , respectively, which in turn can be produced by neutron irradiation of natural dysprosium and erbium or enriched samples of  $^{156}\text{Dy}$  and  $^{162}\text{Er}$ . To produce a high intensity sources one needs a huge amount of irradiated material. For the production of  $^{71}\text{Ge}$  with neutrino intensity of  $2 \times 10^{18} \text{s}^{-1}$  (55 MCi) the 300 kg of natural Ge should be used with the irradiation time of 20 days at the reactor. Obviously, these irradiations in principle can be repeated many times. For the production of  $^{51}\text{Cr}$  ca. 40 kg enriched target of  $^{50}\text{Cr}$  used for GALLEX-detector calibration [13] can be favorably borrowed. The long half-life implies the production of smaller source intensity even after a long-time neutron irradiation, which can not be fully compensated by subsequent long-time data acquisition. Meanwhile, just these long-lived nuclides with the corresponding small neutrino energies can provide as small as possible short oscillation lengths  $L_{32}$ .

The values of  $L_{32}$  in the column 5 were determined by the formula of Eq. (8). Thus we can write:

$$L_{32} = \frac{2.48[\text{m}]E_\nu}{\Delta m_{32}^2([\text{eV})^2} \Rightarrow L_{32}[\text{m}] \approx E_\nu[\text{keV}] \quad (27)$$

The values in the square brackets in Eqs (27) indicate the dimensions used. As can be seen from Table I (column 5) one can roughly divide the nuclides presented there into two categories: those which have  $L_{32} \leq 50$  m and those with  $L_{32} > 110$  m. For the former nuclides the TPC counting method can be used in the gas-filled NOSTOS sphere approach [10], [14], whereas for both and mainly for the latter category with the larger  $L_{32}$ , the long liquid scintillator (LS) detector [15] is more preferable. Both methods are discussed in a forthcoming section. The goal of both approaches is to scan the monoenergetic neutrino-electron scattering events by measuring the electron recoil counts in a function of distance from the neutrino source prepared in advance at the reactor/s. This scan means point-by-point determination of scattering events along the detector dimensions within its position resolution. In the best cases these events can be observed as a smooth curve which reproduces the neutrino disappearance probability. We call this measurement a "neutrino oscillometry". It is worthwhile to note again that the oscillometry is suitable for monoenergetic neutrino since, then, one deals with a single oscillation length  $L_{32}$ . This is obviously not a case for antineutrino, since, in this instance, one extracts only an effective oscillation length. Thus some information may be lost due to the folding with the continuous neutrino energy spectrum.

## EXPERIMENTAL APPROACHES TOWARDS NEUTRINO OSCILLOMETRY

One could propose different experimental methods, already mentioned above, which can be carried out for the scan of neutrino scattering events. One suggestion is to install the neutrino source in the centre of sphere and to measure the events in the  $4\pi$ -geometry which provides the highest angular efficiency, leading to the geometric factor  $g_s = 1$  as discussed above. This, however, is only suitable for relatively small  $L_{32}$ -values because the sphere dimensions are limited, at least very large TPC spheres are not presently available. Another method concerns to the use of long detector (cylinder type) with installation of the source on the top and/or the bottom of detector. Though angular efficiency is much smaller than in the case of sphere,  $g_c \ll g_s$ , the oscillation path could be much longer. In addition, the neutrino source can be removed each time, if necessary, in order to perform the background measurements or to install a new sample for repeated measurements.

In the calculations of the expected number of events for both these methods one needs to know the neutrino intensity of a specific source (see Table I) and the neutrino-electron elastic scattering cross-section. The dependence of this cross-section on neutrino energy is not sensitive to the elemental

TABLE I: Possible candidates for neutrino box-oscillometry. Only the nuclides with half-lives shorter than  $10^5$  y and with the neutrino production intensity higher than  $10^{12}$  s $^{-1}$  have been chosen.

Nuclide	$T_{1/2}$	$Q_\epsilon$ (keV)	$E_\nu$ (keV)	$L_{23}/2$ (m)	$E_{e,max}$ (keV)	weight gr	$\nu$ - intensity(s $^{-1}$ )
$^{41}\text{Ca}$	$10^5\text{y}$	421	417	208	260	400	$10^{12}$
$^{51}\text{Cr}$	28d	753	747	373	560	250	$10^{18}$
$^{55}\text{Fe}$	2.7y	232	226	110	106	4000	$5 \times 10^{17}$
$^{71}\text{Ge}$	11d	232	222	110	100	300	$2 \times 10^{18}$
$^{103}\text{Pd}$	17d	543	480	240	315	15	$5 \times 10^{16}$
$^{109}\text{Cd}$	460d	214*	101	50	30	50	$5 \times 10^{15}$
$^{139}\text{Ce}$	138y	113*	74	37	20	1.5	$2 \times 10^{14}$
$^{157}\text{Tb}$	70y	60.0(3)	9.8	5	0.4	5	$2 \times 10^{14}$
$^{163}\text{Ho}$	4500y	$\approx 2.6$	$\approx 0.5; \approx 0.8$ $;\approx 2.2; \approx 2.3$ 2.6	0.2-1.3	$\leq 0.03$	250	$5 \times 10^{12}$
$^{193}\text{Pt}$	50y	568.0(3)	44(70%) 54(30%)	22 27	6.5 9	300	$5 \times 10^{14}$

composition of the detector's target material and is shown in Fig. 1 for the energy interval up to 750 keV.

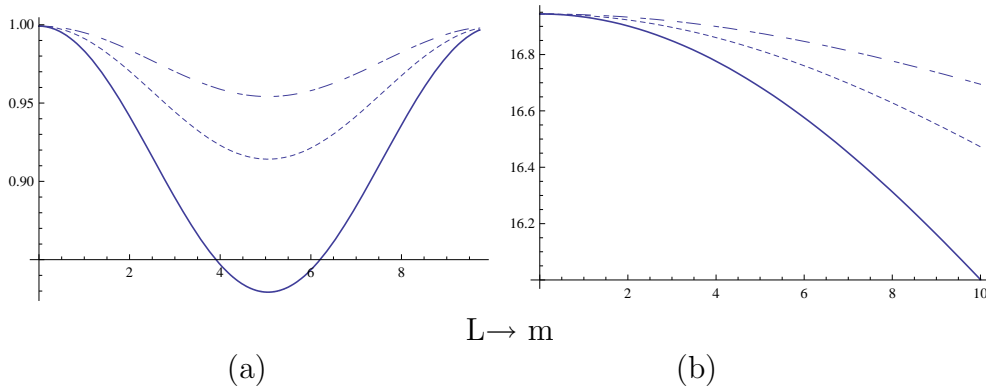


FIG. 3: The rate  $\frac{dN}{dL}$  (per meter) for Ar at 10 Atm with 1 Kg of  $^{157}\text{Tb}$  (a) and  $^{193}\text{Pt}$  (b) as a function of the source-detector distance (in m). The results shown correspond to  $\sin^2 2\theta_{13} = 0.170, 0.085$  and  $0.045$  (decreasing from bottom to top). This rate was obtained for a running period equal to the half life of the source.

### Spherical gaseus TPC-detector with the internal monoenergetic neutrino source

In this spherical chamber the neutrino source is proposed to be situated in the centre of the sphere and the electron detector is also placed around the source in the smaller sphere with radius  $r = 0.5$  m. The sphere volume out of the detector position is filled with a gas (a noble gas such as Ar or preferably Xe, which has a higher number of electrons). The recoil electrons are guided by the strong electrostatic field towards the Micromegas-detector [14],[16]. The NOSTOS, Time Projection Counter, has an advantage in precise position determination (better than 0.1 m) and in detection of very low electron recoils (down to a few hundred of eV, that suits to all nuclides from Table I except of  $^{163}\text{Ho}$ ).



We have seen that the number of electron events is given by Eq. 17. This includes:

- The elastic neutrino-electron cross section.  
(see Eqs 12 and 13). The scale is set by the value given in Eq. 3
- The number of neutrinos emitted by 1 Kg of the source.

$$N_\nu = \frac{m_s}{1 \text{ Kg}} \frac{1}{A_s \times 1.66 \times 10^{-27}} = \frac{m_s}{1 \text{ Kg}} \frac{6.0}{A_s} \times 10^{26} \quad (28)$$

where  $A_s$  is the atomic number of the source and  $m_s$  is its mass. For any given time  $t$  the number of neutrinos emitted must be multiplied by the fraction  $1 - e^{-t/\tau}$  with  $\tau = \frac{T_{1/2}}{\ln 2}$ .

- The number of electrons present in the target:  
Assuming that we have a gas target under pressure  $P$  and temperature  $T_0$  we find:

$$n_e = Z \frac{P}{kT_0} = 4.4 \times 10^{27} m^{-3} \frac{P}{10 \text{ Atm}} \frac{Z}{18} \frac{300}{T_0} \quad (29)$$

( $Z$  the atomic number).

By using this value, as well as the neutrino intensity and the neutrino-electron cross section (see Fig. 1), we estimated the expected total neutrino scattering events as a function of distance from the centre of sphere, for sources  $^{193}\text{Pt}$  and  $^{157}\text{Tb}$ , including the oscillation effect. Here we assumed that the sphere radius was equal to  $r=10$  m and the Ar target was under pressure  $P=10$  Atm at room temperature. We have considered three values of the parameter  $\sin^2(2\theta_{13})$ , namely  $\sin^2(2\theta_{13}) = 0.170, 0.085, 0.045$ . These values were chosen in accordance with the estimate of  $\sin^2\theta_{13} = 0.02 \pm 0.01$  recently obtained [17].

The obtained results are shown in Figs 3a and 3b. In these plots one should pay attention not only to the absolute value of the rate but also to the dip due to oscillation. Clearly very accurate measurements are needed. From the length of oscillation point of view the ideal choice is  $^{157}\text{Tb}$ , since the full oscillation takes place inside the detector, but  $^{193}\text{Pt}$  could be a good compromise.

### Cylindrical detector with the external monoenergetic neutrino source

An alternative approach consists in using a long cylinder filled with a liquid target, which can provide much longer scanning length. Since the liquid target has higher density than a the gaseous one of the spherical TPC, one expects higher event rates. Admittedly, however, for an external target installed on the top of the detector, there will be flux losses caused by smaller effective acceptance angle, if the whole range of length  $L$  is to be explored. This will be especially true for large  $L$ , in which case the cone with the vertex at the place of source will be smaller than a half sphere, let alone a full sphere. As a matter of fact we have seen that the geometric factor, compared to that of a half sphere, is smaller (see Fig. 2). These losses are in some sense compensated by the possibility to scan the long  $L_{32}$ -values which are attributed to relatively short-lived nuclides, which results to higher neutrino source intensities that can be produced (see Table I).

The use of an external and reproducible source has very big advantage because allows to measure the background when source is taken away. This background for the proposed experiment can be generated by cosmic and partly by geo-neutrinos. As an example one can estimate the neutrino scattering rates for the cylindrical detector LENA [15] which can be filled by liquid scintillator in the tank with the diameter 30 m and height 90 m. The parameters of this detector allow to reach the expected position resolution of ca. 60 cm and the energy resolution of 40 keV for 200 keV energy. The best cosmic background conditions are reached at 700 keV energy for the LENA-detector. Therefore in Table I we include the  $^{51}\text{Cr}$  with the neutrino energy 747 keV with a correspondingly long oscillation length in comparison to the length of detector (90 m). One may be able to cope with this problem by satisfying oneself with only a portion of the oscillation inside the detector. The

strong source of  $^{51}\text{Cr}$ , of at least 30 MCi, can be prepared for this case. Figs 5- 8 show estimated total rates for the electron-neutrino scattering for sources  $^{51}\text{Cr}$ ,  $^{55}\text{Fe}$ ,  $^{71}\text{Ge}$  and  $^{103}\text{Pd}$  for the above values of  $\sin^2(2\theta_{13})$ . In estimating the value of  $\Lambda$  the electron density of  $n_e = 2 \times 10^{29}\text{m}^{-3}$  for LS-LAB will be used.

In this case the presentation of the results is more complicated, since the total rate, for a given neutrino energy, depends on two variables  $\rho$  and  $\zeta$  (see Eq. (21)) and the geomtric factor is a bit complicated. We will present our results in units of  $\Lambda = \frac{G_F^2 m^2}{2\pi} N_\nu n_e R$  (see Eq. (23)). Thus only the dependence on the neutrino energy and the geometry will be exhibited.

Naively one might expect to see the oscillation patter in the case of cylindrical geometry directly from the raw data in a fashion analogous to that of the sphere. This naive view, however, is not true as seen in Fig. 4. The variation of the neutrino flux from point to point outweighs the variation of the oscillation amplitude from point to point. Clearly a much more careful analysis should be employed. This is indeed achieved by counteracting the effects of the flux variation, i.e. by multiplying the event rate by  $(\zeta^2 + u^2\rho^2)$ . This way we obtain results as follows:

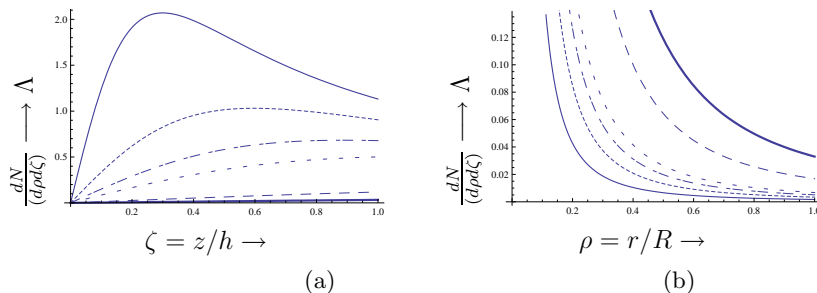


FIG. 4: The differential event rate  $\frac{dN}{d\rho d\zeta}$ , in units of  $\Lambda$  (see text), for a cylinder of radius  $r = 15\text{m}$  and length  $h = 90\text{m}$  and  $E_\nu = 226\text{keV}$ . On the left panel (a) the plots are presented as a function of  $\zeta = z/h$  for the values of  $\rho = r/R = (0.05, 0.1, 0.15, 0.2, 0.5, 1.0)$ , to be read from top to bottom. On the right (b) the same quantity is presented as a function of  $\rho = r/R$  for the values of  $\zeta = z/h = (0.05, 0.1, 0.15, 0.2, 0.5, 1.0)$ . The effect of oscillation is not visible. It is included only for orientation purposes, i.e. to demonstrate that a more careful analysis is needed.

- Rates for the source  $^{55}\text{Fe}$  (neutrino energy 226 keV):  
In this case from the data of table I and the above value of  $n_e$  we obtain  $\Lambda = 0.243\text{s}^{-1} = 7.7 \times 10^6\text{y}^{-1}$ .  
If we multiply the obtained event rate by the above mentioned factor,  $(\zeta^2 + u^2\rho^2)$ , we get the results shown in Fig. 5- 8. From Fig. 5 we see that the magnitude of the rate depends strogly on the radial distance from the axis, but the oscillation period depends only mildly on it.
- Rates for the source  $^{51}\text{Cr}$  (neutrino energy 747 keV).  
In this case  $\Lambda = 0.577\text{s}^{-1} = 1.82 \times 10^7\text{y}^{-1}$
- Rates for the source  $^{71}\text{Ge}$  (neutrino energy 222 keV).  
In this case  $\Lambda = 1.266\text{s}^{-1} = 4.0 \times 10^7\text{y}^{-1}$
- Rates for the source  $^{103}\text{Pd}$  (neutrino energy 480 keV).  
In this instance  $\Lambda = 0.0282\text{s}^{-1} = 891\text{y}^{-1}$

It is rewarding that, if the data analyzed as above, the oscillation pattern exhibited by a cylindrical detector is not very different from that of the spherical detector. It should be kept in mind that the exhibited range of  $\zeta$  is to guide the eye. The maximum value of  $\zeta$  is, by definition, unity.

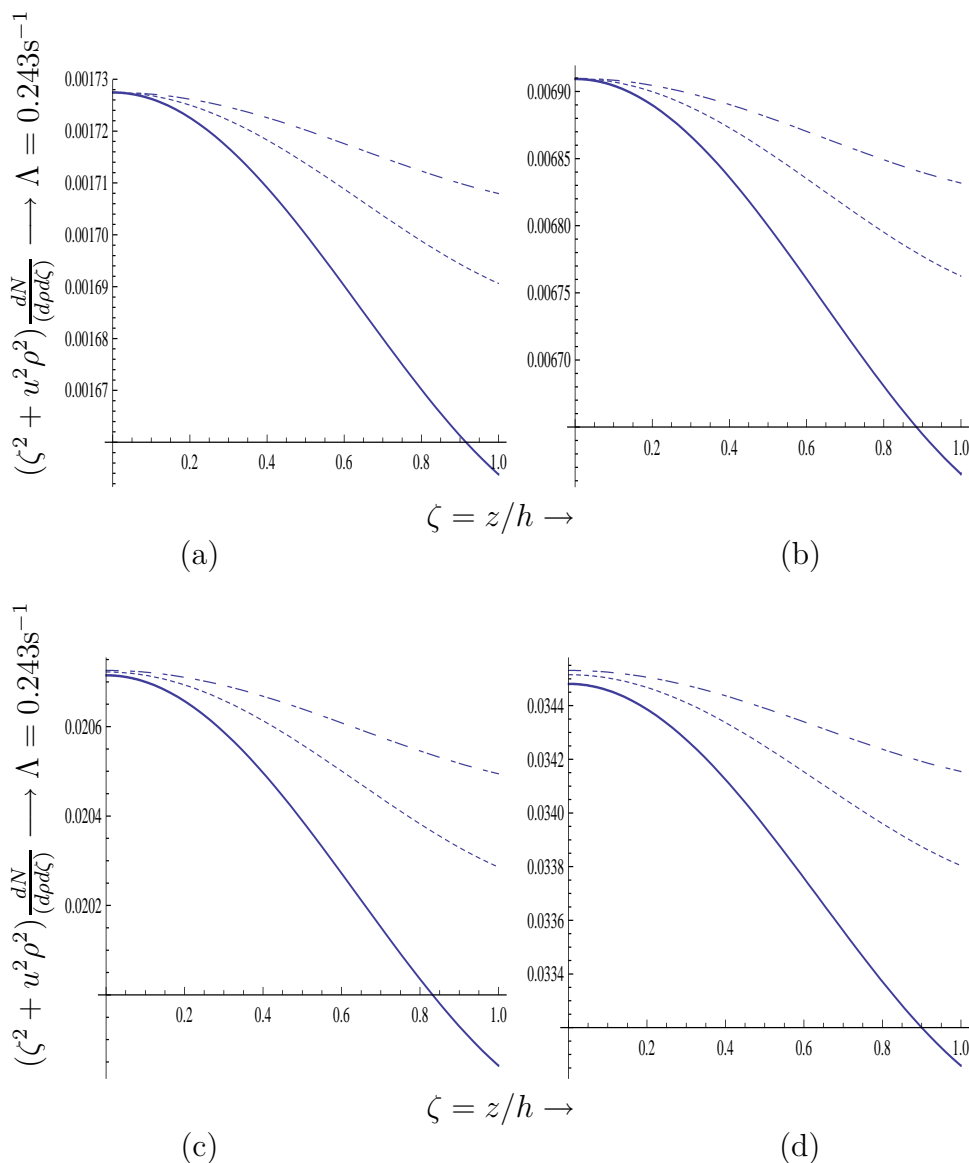


FIG. 5: The differential event rate  $(u^2 \rho^2 + \zeta^2) \frac{dN}{d\rho d\zeta}$  (in units of  $\Lambda$ ) for a cylinder of Radius  $R = 15\text{m}$  and length  $h = 90\text{m}$  as a function of  $\zeta = z/h$  for  $^{55}\text{Fe}$  ( $E_\nu = 226\text{ keV}$ ). The solid, dotted and dashed curves correspond to  $\sin^2 2\theta_{13} = 0.170, 0.085$  and  $0.045$  respectively. The panels (a), (b), (c), (d) correspond to values of  $\rho = r/R = 0.05, 0.2, 0.6$  and  $0.8$  respectively.

#### Analysis of the data of a cylindrical detector in terms of $L$

In the previous section we analyzed the data by obtaining the event rate for each point  $\rho, \zeta$  of the detector. One may attempt to present the data in terms of the source detector distance  $L$  by a suitable transformation from the variables  $(r, z)$  to  $(L, \phi)$  and integrating over the angle  $\phi$ . A tedious but straightforward algebra yields:

$$R \frac{dN}{dL} = N_\nu n_e R \frac{1}{2} g_{\text{av}}(u, L/R) \sigma(E_\nu, L) = \Lambda \frac{1}{2} g_{\text{av}}(u, L/R) \tilde{\sigma}(E_\nu, L) \quad (30)$$

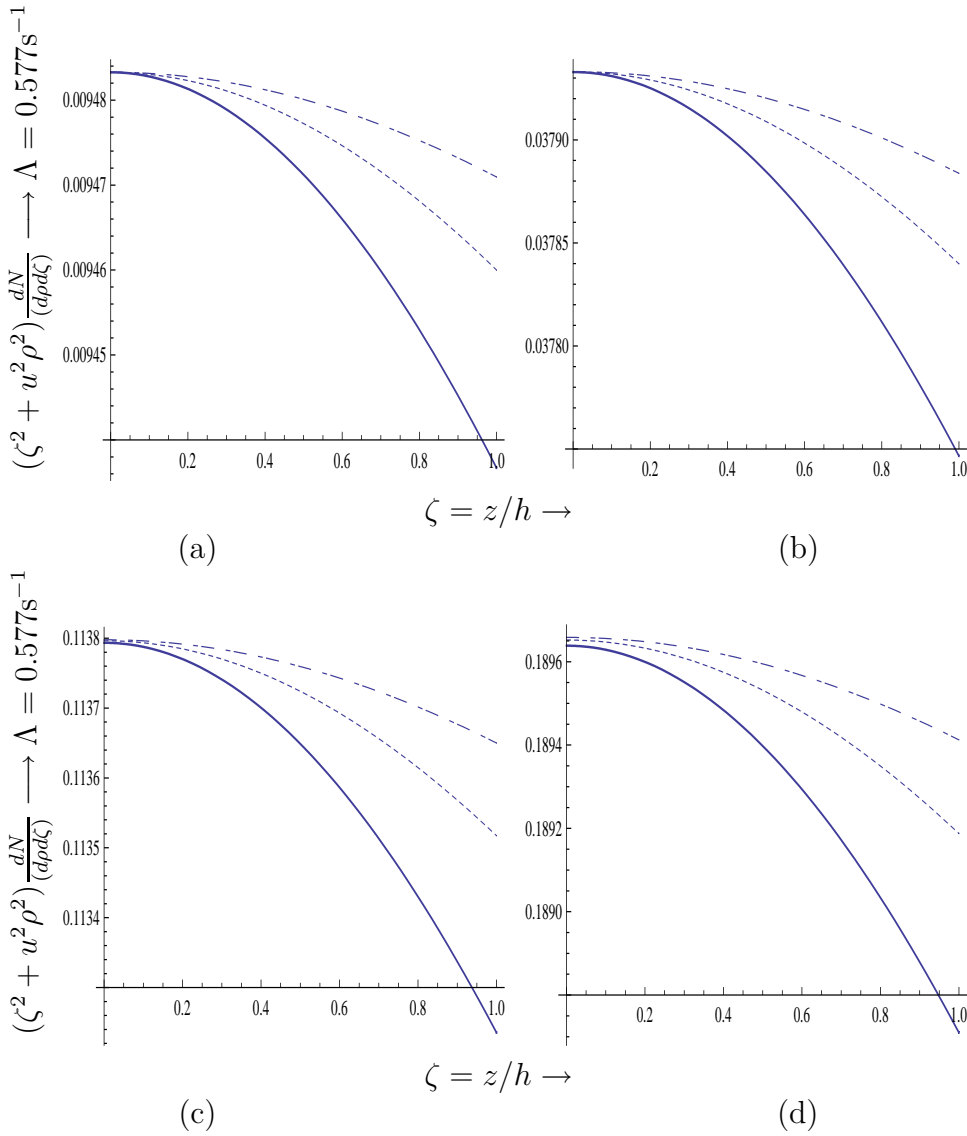


FIG. 6: The same as in Fig. 5 for  $^{51}\text{Cr}$  ( $E_\nu = 747$  keV).

where  $g_{\text{av}}(u, L/R)$  is a geometric factor that takes care of the variation of the neutrino flux in the various positions described by  $L$ . It can be cast in the form:

$$\begin{cases} 1, & 0 < v < 1 \\ g_{\text{av}}(u, v) = 1 - \sqrt{v^2 - 1}/v, & 1 < v < 1/u \\ (1/u - \sqrt{v^2 - 1})/v, & 1/u < v < \sqrt{1 + 1/u^2} \end{cases} \quad (31)$$

This function for  $u = 1/6$  is shown in Fig. 9. On the same figure we show the expected event rate for a typical case like  $^{55}\text{Fe}$ . It is clear that to disentangle the oscillation dependence on  $L$  one must divide the expected rate by the geometric factor. When this is done we obtain the results shown in Figs 10 and 11.

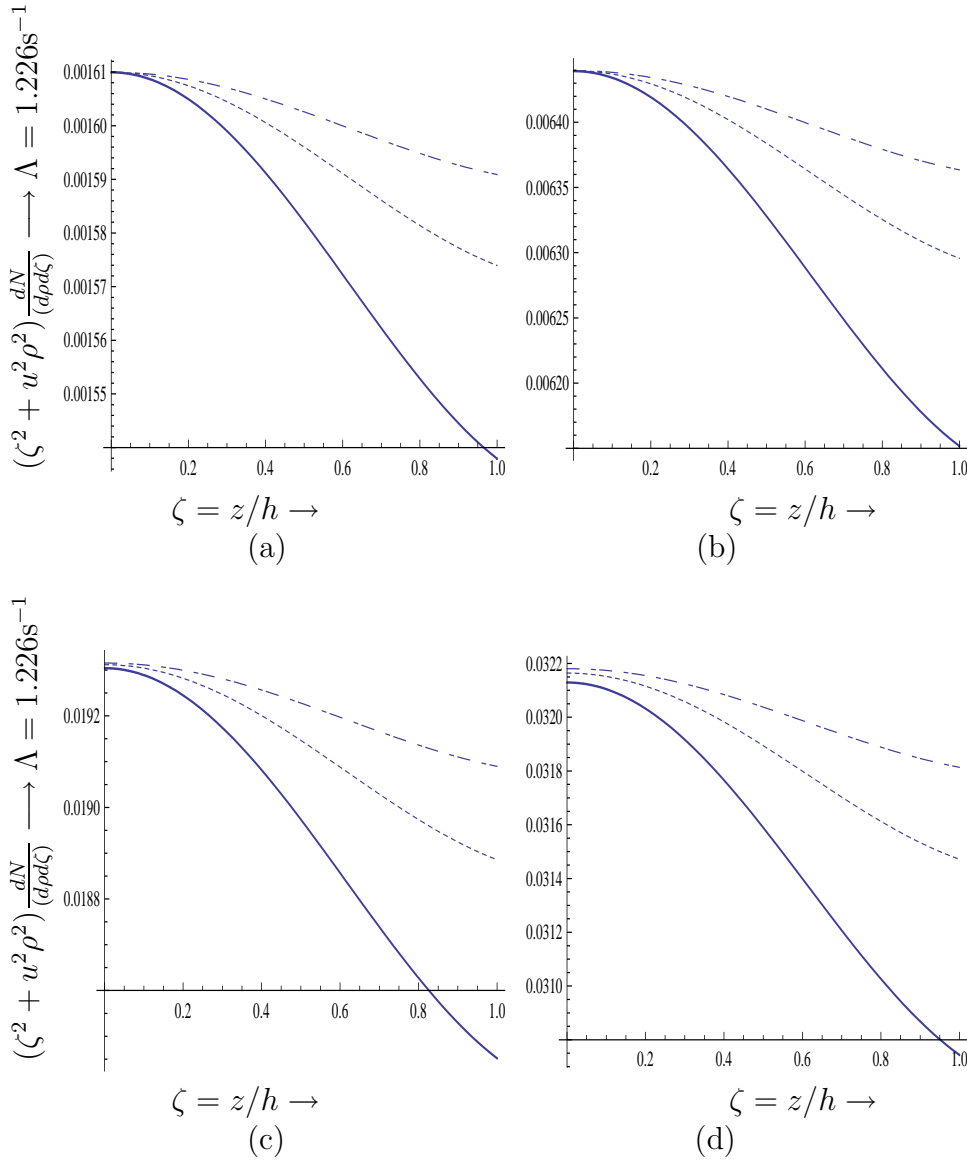


FIG. 7: The same as in Fig. 5 for  $^{71}\text{Ge}$  ( $E_\nu = 222$  keV).

## DISCUSSION

In this article we consider two possible experimental approaches for the neutrino oscillometry: the spherical gaseous detector and the liquid scintillator cylindrical one. Both cases have their own advantages and disadvantages.

- The spherical gaseous detector.

This requires the construction of a sphere with the radius much larger than 10 meters can hardly be built. This restricts the possible candidates for the neutrino oscillometry by nuclides whose neutrinos energies should not be much higher than 10 keV in accordance with the equation 27. The relevant oscillometry curves are shown in Fig. 3 employing an Ar gas. One kg of source, installed at the center of the sphere, was employed under the assumption of a time measurement longer than the half-life of the source. To obtain the number of events collected

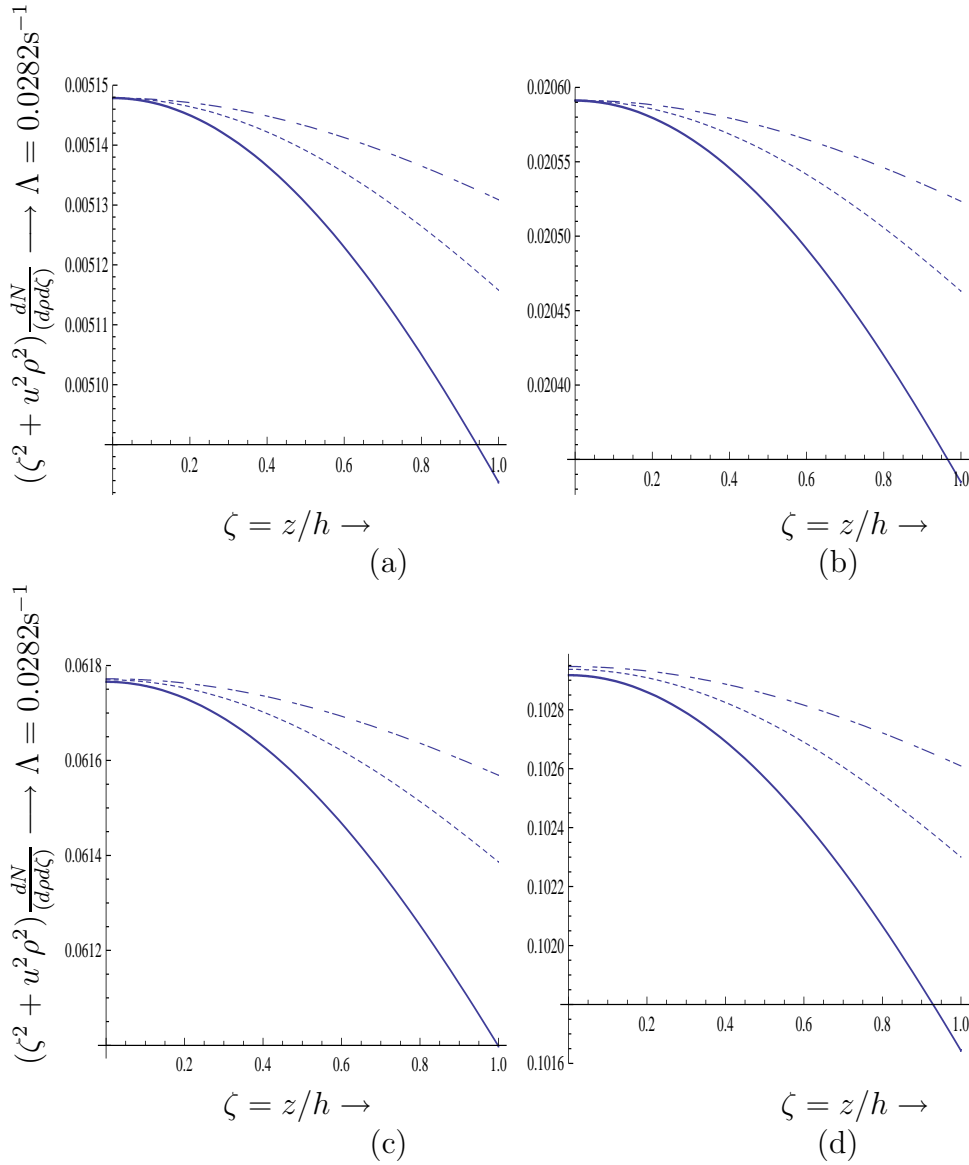


FIG. 8: The same as in Fig. 5 for  $^{103}\text{Pd}$  ( $E_\nu = 480$  keV).

during the reasonable measurement time, the values in Figs 3 must be multiplied by a number of disintegrated nuclides during this time. Thus, e.g., for one year measurement with the 0.15 kg of  $^{157}\text{Tb}$  one can obtain the rate equal approximately to  $8 \times 10^{-4}$  events per meter, too low value. The similar feature is expected for other relatively weak neutrino emitters listed in the bottom part of Table I. Thus we can conclude that the spherical gaseous detector with the neutrino source in the center, being very attractive in its idea, cannot provide presently the appropriate conditions for neutrino oscillometry. As a matter of fact, the requirement of low energy neutrinos brings the long-lived candidates with the low rate of events. The small neutrino energy is associated with the tiny neutrino-electron cross-section, and the small electron recoil energy requires the use of gaseous environment with the TPC-detection which has not a high target electron density. All these disadvantages with an additional demands for very long irradiation at the reactor for the production of appropriate nuclides and a very long data acquisition time makes this approach very problematic.

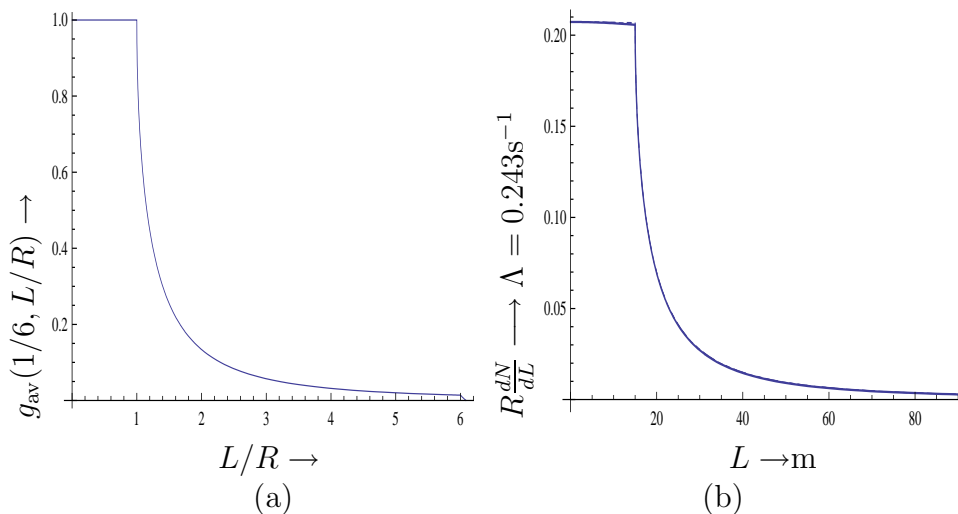


FIG. 9: In panel (a) we show the geometric factor  $g_{av}(1/6, L/R)$  as a function of  $L/R$  for the value  $u = R/h = 1/6$ . Note the flux factor of  $1/2$  has explicitly put in in Eq. (30) and thus it is not included in the geometry. In the first region, which is a spherical segment, one sees that the geometric factor is unity like the case of the sphere. In panel (b) we show the expected event rate (in units  $\Lambda = 0.243\text{s}^{-1}$ ) in the case of the  $^{55}\text{Fe}$  source as a function of  $L$  in meters. It is obvious that both plots follow the same pattern.

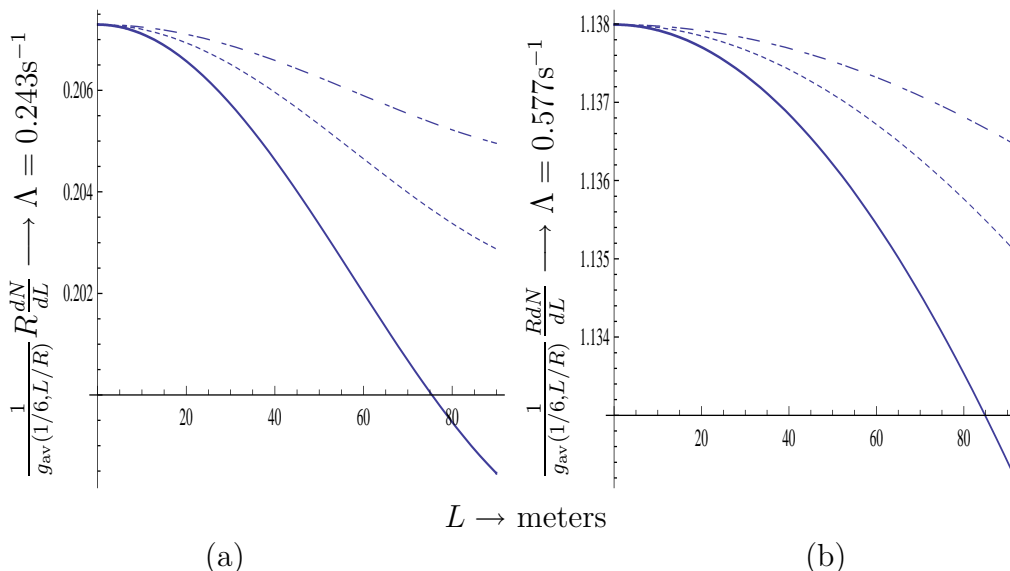


FIG. 10: In panel (a) we show the expected event rate  $R \frac{dN}{dL}$ , divided by the geometric factor, in units of  $\Lambda = 0.243\text{s}^{-1}$  expected for the source  $^{55}\text{Fe}$ , while in panel (b) we show the same quantity for  $^{51}\text{Cr}$  in units of  $\Lambda = 0.577\text{s}^{-1}$ . In both panels the solid, dotted and dashed curves correspond to  $\sin^2 2\theta_{13} = 0.170, 0.085$  and  $0.045$  respectively. One does not see the full oscillation inside the detector, but the information is adequate to extract useful information on the neutrino oscillation parameters.

- A long cylindrical detector.

In this case the neutrino source in a form of a small sphere can be installed at the top/bottom of the cylinder at the center of the circular face. Even though the angular efficiency of such configuration is much less than for  $4\pi$  acceptance of the spherical detector, there are many

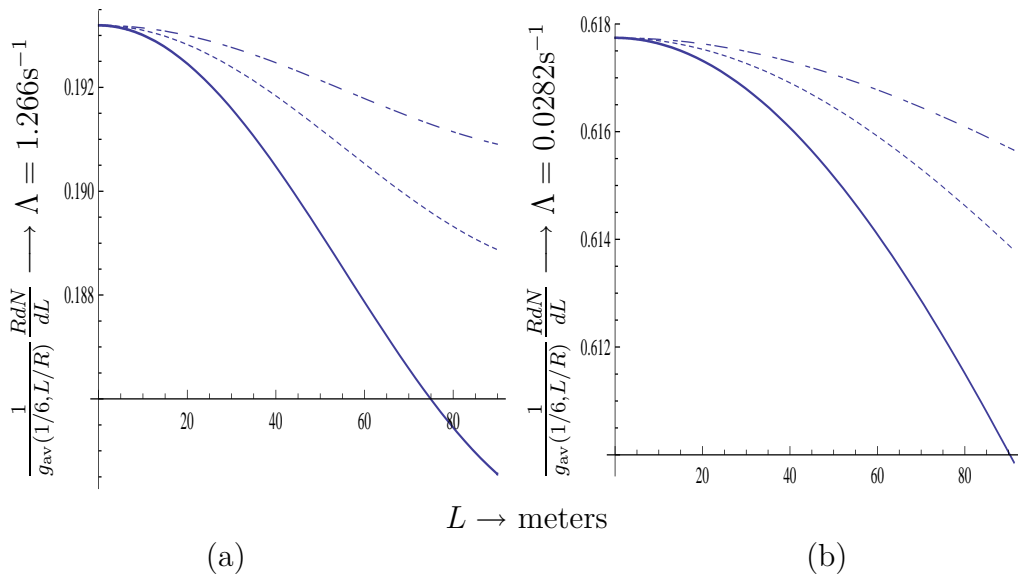


FIG. 11: The same as in Fig. 10 in case of the source  $^{71}\text{Ge}$  (a) and  $^{103}\text{Pd}$  (b).

advantages which overbalance this lack. If the length of cylinder is rather long (let's presume about 100 m) the neutrino emitters with the energies in the hundreds keV region can be used for oscillometry. This on one hand increases the neutrino-electron cross-section (see Fig. 1), while on the other drastically increases the neutrino source decay rate because of decreasing the source half-life. Then the increased in the energy of the recoiling electrons makes possible to use a liquid target, which leads to the increase of the number of target electrons.

As it can be seen from the top part of Table I there are several candidates ( $^{51}\text{Cr}$ ,  $^{55}\text{Fe}$ ,  $^{71}\text{Ge}$ , and  $^{109}\text{Pd}$ ) for whom the neutrino flux is a few order of magnitudes higher than for the heavier nuclides. The  $(\nu_e, e)$  cross-section for, e.g.  $^{71}\text{Ge}$  or  $^{55}\text{Fe}$ , are at least two orders of magnitude higher than that for  $^{157}\text{Tb}$ , a typical candidate for oscillometric measurements in the spherical gaseous TPC. One-two orders of magnitude can be won for electron density in the liquid target. Thus, approximately eight orders of magnitude gain for a long cylindrical liquid detector is against about of one-two orders of magnitude angular efficiency loss in comparison to spherical gaseous case. Meanwhile, there is some disadvantage in the use of cylinder whose length is restricted by 100 m or a little bit more. For relevant candidates collected in the I with the neutrino energy higher than 220 keV the scan in a full oscillation length (including both disappearance and appearance events) is impossible. Meanwhile, as it can be seen from Fig. 5, the oscillation curves can be well recognized (till  $z/h=1$ ) and the dependence on the mixing angle  $\theta_{13}$  is also visible.

In order to show the feasibility of neutrino oscillometry for long cylindrical liquid target let's comment the curves in Fig. 5. These curves have been calculated for the neutrino energy of 226 keV in the cylinder with the length  $h = 90\text{m}$  and with the radius  $R = 15\text{m}$  filled by the liquid scintillator (LS). The scale parameter  $\Lambda = 0.243\text{s}^{-1}$  appearing in these curves can be obtained with assumption that the neutrino source intensity is  $N_\nu = 5 \times 10^{17} \text{ s}^{-1}$  (see Table I) and an electron density  $2 \times 10^{29} \text{ m}^{-3}$  via Eq. 23. As a factor  $u^2 \rho^2 + \eta^2 = (r^2 + z^2)/h^2$  it is less than 1 for practically full neutrino path in the cylinder, the range of values of the average differential rate,  $\partial^2 N / \partial \rho \partial \zeta$ , is from  $> 10^{-3} \text{ s}^{-1}$  for the top left curves of Fig. 5 to  $> 2 \times 10^{-2} \text{ s}^{-1}$  for the bottom right ones. The values of differential accounts strongly depend on the  $(r, z)$ -position of event in the cylinder. Another evidence for successful oscillometry can be shown from the presentation of the data in the  $\partial^2 N / \partial \rho \partial \zeta$  -values. Though the expected position resolution in the cylinder with LS is better [15] than 1 m, we will assume the volume resolution equal to  $1 \text{ m}^3$ . Fig. 5 shows an experimental



”fingerprint” which is expected from the existence of neutrino oscillations.

The solar neutrino background depends on the energy region of interest and it becomes small above 400 keV. The expected background from the solar events in this region is  $< 1 \text{ day}^{-1} \text{m}^{-3}$  for an LS detector of the size used in our calculations. It is thus useful to obtain some oscillation features in this energy region, using the two sources  $^{51}\text{Cr}$  and  $^{103}\text{Pd}$ , which are favorable in this region. The oscillation features of these nuclides are shown in Figs 6 and 8. One can obtain at the end of the cylinder a difference of  $8.7 \times 10^{-3} \text{Rs}^{-1}$  for values  $\sin^2 2\theta_{13} = 0.170$  and  $0.045$  in the case of  $^{51}\text{Cr}$ . This yields  $5.8 \times 10^{-4} \text{m}^{-1} \text{s}^{-1}$ . Taking into account the radioactive decay of  $^{51}\text{Cr}$  we obtain 1560 events per meter for 60 days of measurement. This difference exceeds the  $4\sigma$  standard statistical uncertainty, even for this unfavorable candidate. Note that the estimated rates in the liquid scintillator presented in Fig. 6 are higher than expected background mentioned above.

More impressive results are expected in the case of  $^{55}\text{Fe}$  and  $^{71}\text{Ge}$ , which are characterized by the fact that almost the full oscillation takes place inside the detector (see Figs 5 and 7 as well as 10 and 11). We should mention, however, that in this energy one encounters higher solar neutrino background [18].

Quite high values obtained can be even increased if the data handling is going during several months or even weeks. These measurements can be stopped in any time. Source can be moved and new source installed. Because of high neutrino intensity the reasonable result can be obtained very quickly without the agonizing long-term measurements. This advantage of removable sources is indeed very attractive.

## CONCLUSIONS

The new method for neutrino oscillation measurements is proposed. It is based on the use of monoenergetic low energy neutrinos which are released in the atomic electron capture by nuclei. High intensity neutrino sources with the neutrino energies less than a few hundreds keV can be produced in neutron reactors. They can be installed at the top of the long cylinder filled by liquid target material or placed in the center of gaseous sphere placed underground. The measurement consists in finding the number of events arising from the electron neutrino scattering on the electrons of the target. It was shown that, for some appropriate candidates like ( $^{55}\text{Fe}$ ,  $^{71}\text{Ge}$ ,  $^{109}\text{Cd}$ ), the so called small oscillation length  $L_{32}$  can fall within the dimensions of cylindrical detectors which can be constructed in the nearest future. There the oscillations can be determined by disappearance of events caused by the change of the neutrino flavor just inside the detector. These events can be scanned point-by-point thus providing the oscillometry curve. The calculations for the cylindrical detector with the length  $h = 90 \text{ m}$  and radius  $R = 15 \text{ m}$  showed a complicated net of events which can be analyzed by the ”oscillation signature” suggested. The most attractive advantage of proposed experiment is the possibility to move the neutrino source, to measure the background or to implement other physics project and also to replace one source by another. With the neutrino source intensity of 30 MCi, which provides high count/background rate, the observation of oscillations can be performed during months or even weeks in underground conditions. Since the  $\theta_{13}$  discovery potential for proposed experiments spans the values of  $\sin^2 2\theta_{13} < 0.170$ , the experiments with low monoenergetic neutrinos, e.g., with the LENA-detector, could be complementary to investigations with the reactor and accelerator neutrinos in Double Chooz, RENO, Daya Bay, T2K and NOvA projects planned for the coming decade. The physics interest in the short baseline oscillometry measurements is not only the determination of  $\theta_{13}$ . The discovery of the  $L_{32}$  -value from the oscillometry experiments with the subsequent comparison with the electron neutrino energy will allow to check availability of equation (27), the dynamics of  $\nu_e - e$  low energy interactions and, in general, the validity of the long baseline oscillation results obtained so far. The present analysis does not suffer from the 8-fold degeneracy [19] that corrupts the measurement of  $\theta_{13}$  in conventional long-baseline experiments. The neutrino energies, needed to check (27), can be accurately determined by independent direct mass measurements of nuclides, a capture-partners, in the ion traps [11].

acknowledgments: This work was supported in part by the European Union under the contract MRTN-CT-2004-503369 and by the program PYTHAGORAS-1 of the Operational Program for

Education and Initial Vocational Training of the Hellenic Ministry of Education under the 3rd Community Support Framework and the European Social Fund. Support by the Russian ministry of science is also acknowledged.

We would also like to thank Y. Giomataris and A. Vasiliev for their very fruitful remarks and discussions. Fruitful discussions during the preparation of this work with Ya. Azimov, E. Akhmedov, K. Blaum, S. Eliseev, T. Enqvist, A. Erikalov, F. von Feilitzsch, W. Hampel, V. Isakov, H.-J. Kluge, U. Koester, M. Lindner, K. Loo, A. Merle, T. Oberauer, W. Trzaska, J. Winter, M. Wurm, and A. A. Vorobyov are also happily acknowledged.

- 
- [1] Y. Fukuda *et al*, The Super-Kamiokande Collaboration, *Phys. Rev. Lett.* **86**, (2001) 5651; *ibid* **81** (1998) 1562 & 1158; *ibid* **82** (1999) 1810; *ibid* **85** (2000) 3999.
- [2] Q.R. Ahmad *et al*, The SNO Collaboration, *Phys. Rev. Lett.* **89** (2002) 011302; *ibid* **89** (2002) 011301; *ibid* **87** (2001) 071301.  
K. Lande *et al*, Homestake Collaboration, *Astrophys. J* **496**, (1998) 505  
W. Hampel *et al*, The Gallex Collaboration, *Phys. Lett. B* **447**, (1999) 127;  
J.N. Abdurashitov *al*, Sage Collaboration, *Phys. Rev. C* **80** (1999) 056801;  
G.L Fogli *et al*, *Phys. Rev. D* **66** (2002) 053010.
- [3] K. Eguchi *et al*, The KamLAND Collaboration, *Phys. Rev. Lett.* **90** (2003) 021802, hep-exp/0212021.
- [4] J. N. Bahcall, M.C. Gonzalez-Garcia, and C. Peña-Garay. *JHEP*, 0302:009, 2003. (hep-ph/0212147).
- [5] V. Barger and D. Marfatia. *Phys. Lett. B*, 555:144, 2002. (arXiv:hep-ph/0212126).
- [6] G. 't Hooft. *Phys. Lett. B*, 37:195, 1971.
- [7] F. Reines, H.S. Gurr, and H.W. Sobel. *Phys. Rev. Lett.*, 6:315, 1976.
- [8] P. Vogel and J. Engel. *Phys. Rev.*, D 39:3378, 1989.
- [9] G.J. Gounaris, E.A. Paschos, and P.I. porfyriadis. *Phys.Rev. D*, 70:113008, 2004.
- [10] Y. Giomataris and J.D. Vergados. *Nucl. Instr. Meth. A*, 530:330, 2004.
- [11] K. Blaum, Yu.N. Novikov, and G. Werth. *Contemp. Phys.*, 51:149, 2010. [arXiv:0909.1095](physics.atom-ph).
- [12] F. Larkins. *At. Data and Nucl. Data Tables*, 20:311, 1977.
- [13] W. Hampel *et al*. *Phys. Lett. B*, 420:114, 1998.
- [14] Y. Giomataris *et al*. *Nucl. Instr. and Meth. A*, 376:29, 1996.
- [15] L. Oberauer, F. von Feilitzsch, and W. Potzel. *Nucl. Phys. B*, 138:108, 2005.
- [16] I. Giomataris *et al*. *JINST*, 3:P09007, 2008. arXiv:0807.2802 (physics.ins-det).
- [17] G. Fogli *et al*, arXiv: 0905.3549v2[hep-ph].
- [18] J.N. Bahcall and R.K. Ulrich. *Rev. Mod. Phys.*, 60:297, 1988.
- [19] V. Barger, D. Marfatia, and K. Whisnant. *Phys. Rev. D*, 65:073023, 2002; [hep-ph/0112119].

